Scholars Journal of Engineering and Technology
Abbreviated Key Title: Sch J Eng Tech
ISSN 2347-9523 (Print) | ISSN 2321-435X (Online)
Journal homepage: https://saspublishers.com

Computational Fluid Dynamics Analysis of Underexpanded, Fully-Expanded and Overexpanded Supersonic Jets Emanating from A Convergent-Divergent Nozzle

R. C. Mehta[1*]

[1]Department of Aeronautical Engineering, Noorul Islam Centre for Higher Education, Kumaracoil 629180 India

DOI: https://doi.org/10.36347/sjet.2025.v13i07.008 | **Received:** 12.05.2025 | **Accepted:** 19.07.2025 | **Published:** 22.07.2025

***Corresponding author:** R. C. Mehta
Department of Aeronautical Engineering, Noorul Islam Centre for Higher Education, Kumaracoil 629180 India

Abstract **Original Research Article**

An axisymmetric inviscid numerical study is carried out to obtain free supersonic jet structures of underexpanded, perfectly expanded and overexpanded supersonic jets emanating from a convergent-divergent nozzle having a semi-divergence angle of 15° for exit Mach number M_e = 2.20, 2.61 and 3.12, and nozzle exit to ambient pressure ratio of p_e/p_a = 1.54, 1.36, 1.09 and 0.45. Computer fluid dynamics results include flowfield visualizations of density and Mach contour, pressure distributions along centre line of free jets. Comparison have been made with schlieren photographs to locate Mach disc and shock cell lengths. They are found in good agreement with available experimental results. It is observed that the first shock cell length is a function of exit Mach number, but the second cell is a function of shock strength. Colour schlieren optical technique in conjunction with digital image processing algorithm is initiated to analyse free supersonic jet structure.

Keywords: Convergent-divergent nozzle; Computational fluid dynamics; Inviscid flow; Mach disc; Supersonic jets; Schlieren picture, Shock strength.

INTRODUCTION

The increased concern in the design of turbo-jet, rocket propelled aircraft jet, missiles, rocket engines and solid motor of space launch vehicle has caused a great deal of attention to be focused on the jet flow behind supersonic nozzle. Rocket engines and solid motors are occasionally designed with highly underexpanded nozzles. The large jet plume which results can also affect the aerodynamics in the vicinity of the bases of missiles and satellite launch vehicle.

Supersonic jet emanating from a convergent-divergent nozzle may be underexpanded ($p_e/p_a > 1$) or overexpanded ($p_e/p_a < 1$), correctly expanded ($p_e/p_a = 1$) depending upon the stagnation pressure ratio (P_o/p_a). The basic flow field structure for these cases is obtained by experiment. Generally, it consists of repetitive shock cell structure in the potential core, inviscid jet boundary and a shear layer. In the case of correctly expanded jet, the shock cells consist of weak shock and regular shock reflection. However, for the overexpanded and underexpanded cases, formation of Mach disc takes place.

Love and Lee [1] have calculated size and shape of free jets emanating from a convergent-divergent nozzle having semi-divergence nozzle angle of 15° using method of characteristics for a large value of nozzle pressure ratio and different values of specific ratio of heats (γ = 1.2, 1.4, 1.667) at nozzle Mach number M_j = 2.5. For highly underexpanded case, the flow up to the Mach disc is generally estimated by different numerical schemes such as methods of characteristics [2, 3, 4]. For overexpanded cases, the strong jet shocks from the nozzle forms the Mach disc near to the nozzle exit; hence the estimation becomes difficult. Mehta and Prasad [5] studied the effects of various p_e/p_a ratios on shock-cell lengths with schlieren and density contour plots. The results revealed that the Mach disk moves closer to the nozzle exit plane with decreasing pressure ratio, and the length of the first shock cell decreases. Supersonic gas jets in conical convergent–divergent nozzles are studied numerically using the rhoOpenFOAM software solver [6]. A commercial CFD software ANSYS, FLUENT [7] has been adopted for analysing flow through convergent-divergent nozzle and quantitative data on pressure, velocity magnitude and Mach number.

In 1904 Prandtl [8] developed a pioneering small perturbation theory to obtain the well-known "Prandtl Formula" for the wavelength of an almost perfectly expanded circular supersonic jet, uniform everywhere and notably so on the bounding streamlines. Powell [9] derived a simple loop equation relating to the mechanism's three main components, which are shock cell length, disturbance spacing, and the discrete tone wavelength. The shock associated noise does appreciably for the imperfectly expanded jet [10]. For shock generated noise prediction, it is therefore customary to obtain the shock cell length accurately [11]. A supersonic core length and an average shock-cell length are experimentally investigated [12] for the acoustic properties of supersonic jets. The flowfield of a single jet at correct expansion of Mach 2.0 was studied experimentally [13] using pressure measurement and schlieren flow visualization. They found that the Mach number values along the jet centre line obtained from the pixel intensities using image processing technique from schlieren image are compared with the Mach number values obtained from the computational fluid dynamics.

Abdel-Fattah [14] analysed Mach disc location and shock cell lengths using schlieren picture and a derived correlation for shock cell length. Mehta and Prasad [15] have employed numerically and experimentally shock cell length different nozzle pressure ratios as well as different exit Mach numbers. It is found that the location of Mach disc moves away from the nozzle exit with increase in expansion pressure ratio p_e/p_a. Franquet *et al.,*[16] have presented a review paper on free underexpanded jets in a quiescent medium. Flow structure and parameter evaluation of convergent–divergent nozzle supersonic jet flows have been developed using numerical techniques by Munday *et al.,*[17] and Xiao *et al.,*[18]. A supersonic core length and an average shock-cell length are experimentally investigated for the acoustic properties of supersonic jets. Yu, *et al.,*[19] have been carried out experiment and numerical simulation investigation of free jets on a flat plate at different different nozzle pressure ratios at nozzle exit Mach number 1.88.

Free jet may be considered as a pressure driven unrestricted compressible continuous flow from a convergent-divergent nozzle into a quiescent atmosphere. This action pulls surrounding fluid into jet through the vorticed formed as a result of jet interaction with the ambient fluid. This action is termed as entertainment process. Figure 1 exhibits a schematic sketch of the repetitive shock cell pattern generally generated behind an underexpanded axisymmetric convergent-divergent nozzle (about $p_e/p_a > 3$). As the fluid emanates from the nozzle exist, it passes through an Prandtl-Meyer expansion fan [20], expanding to the ambient at the jet boundary, and then the condition of constant pressure along the jet boundary causses this boundary to be bent back toward the axis of flow. As the flow alters direction along jet boundary, many compression waves, appeared at the interaction of expansion waves with the jet boundary, are sent back into flow, these waves coalesce to form the intercepting shock indicated in the sketch.

The structure of underexpanded jet flows is rich, typically being comprised of an external shock emanating from near the lip of the nozzle; a shear at the jet boundary; an expansion for emanating from the lip of the nozzle; an intercepting shock emanating from the lip of the nozzle; a reflection of the intercepting shock; and for very low back pressure a Mach disc; a slip line emanating from the intersection point of the intercepting shock and Mach disc.

For slightly underexpanded nozzles, these intercepting shocks merge at the axis forming the familiar diamond configuration. As the pressure ratio across the nozzle is increased, however, these intercepting shocks no longer meet at axis but are connected with a Mach disc, as depicted in Fig. 1. In both cases, reflected shocks are formed which intersect with the jet boundary reflecting an expansion wave, and the whole presses is repeated. The repetition is

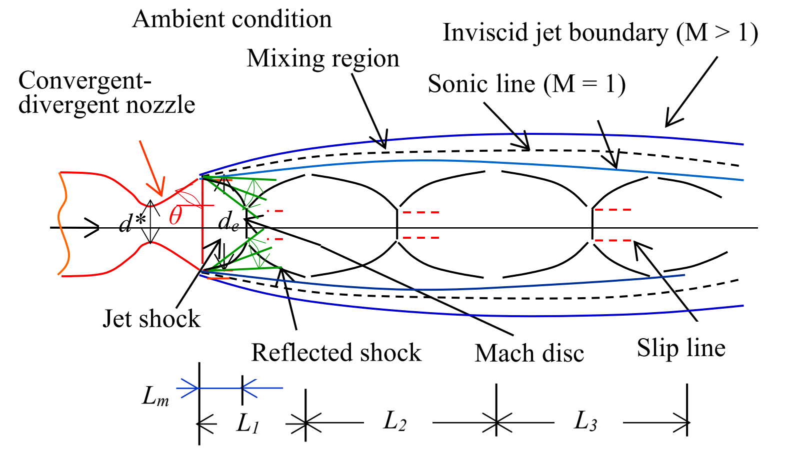

(*a*) Underexpanded ($p_e/p_a > 1$)

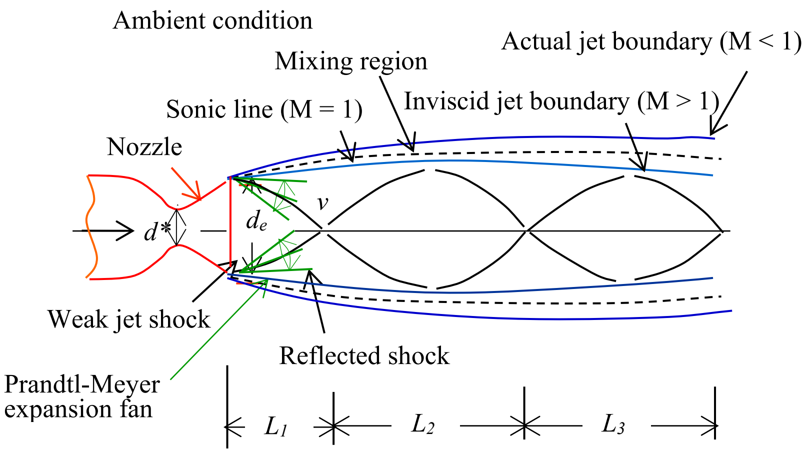

(*b*) Fully expanded, $p_a/p_e = 1$

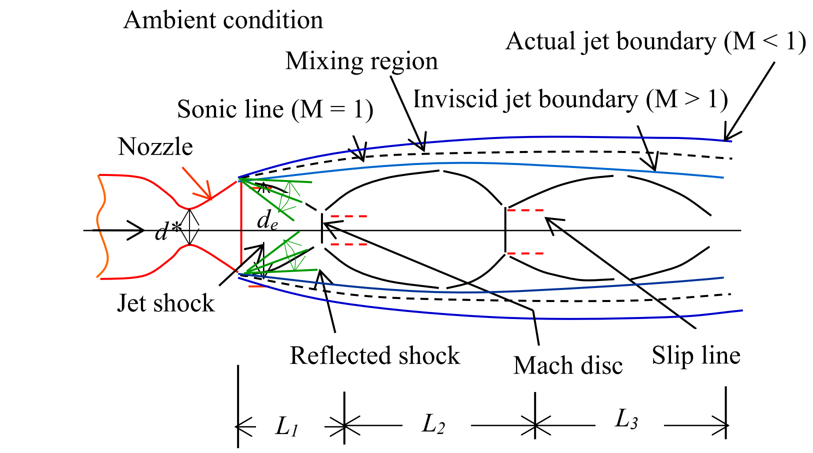

(*c*) Overexpanded ($p_e/p_a < 1$)

Fig. 1: Schematic sketch of free supersonic jets at different pressure ratio (p_a/p_e)

continued until viscous effects become predominant and this structure is no longer observed. Mehta [21] has indicated that for a jet exhausting into a static atmosphere the important parameters are the static pressure ratio at the nozzle exit (p/P_o) the Mach number at the nozzle exit, and to a very slight degree, the divergence angle at the nozzle.

The entrained mass at low momentum tries to gain momentum from the high-speed fluid element in the vicinity of the of the jet centre line. In a jet flowfield, the large-scale structures act as distributors of the mass entrained by the large-scale structure. Because of this the jet velocity begins decreasing downstream of the nozzle exit. The mass flow from the surrounding at any cross section of the jet progressively increases along the downstream direction, thus, the mass conservation is not valid for jet flows. However, the jet has to governs the momentum conservation. Hence, to conserve momentum, the jet centre line velocity decreases with downstream distance. The process of velocity decrease is properly known as the jet decay.

We are considering here moderately underexpanded jet $P_o/p_a < 3.78$ ($1.1 < p_e/p_b < 2$) and highly underexpanded jet $P_o/p_a > 3.78$ emanating from a convergent-divergent nozzle that depends on ratio of P_o to p_a. The interception shock is an oblique shock behind which the flow is still supersonic but at a lower Mach number than the flow in the core of the jet. For moderately underexpanded jets as depicted in Fig. 1(a) these intercepting shocks meet at the axis forming the familiar diamond configuration. Here the term moderately underexpanded is used to denote jets within the pressure interval $1.1 < p_e/p_b < 2$. The form of the shock structure in the initial cell begins to change depending on the P_o/p_a.

The phenomenon of under- and overexpanded supersonic free jets emanating from a convergent-divergent nozzle. When a convergent-divergent nozzle deviates from its operating conditions then semi-periodic shock diamonds and Prandtl–Meyer fans appear in the jet field. However, at the design conditions, the traditional smoothly contoured convergent-divergent nozzle with exit flow is a shock-free condition as shown in Fig. 1 (*b*). If the nozzle exit pressure equal to the back pressure, then the jet is said to be fully expanded $P_o/p_a = 1.89$. This jet is also wave dominated as an imperfectly expanded jet, unlike what we usually think that there will not be any waves. The reason for this is that, as the jet is issuing from the confined area to an infinite area it tries tom expand through expansion waves and after that gets compressed through compression waves, which results in a periodic wave structure. Of course, for this case waves will not be strong as in the case of overexpanded flow. If the pressure in the ambient medium is lower than the nozzle exit pressure, the jet is said to be underexpanded $P_o/p_a > 1.89$. Since the back pressure is less than the nozzle exit pressure, a wedge-shaped expansion fans occur at the edge of the nozzle. These waves cross one another and are reflected from the opposite boundaries of the jet as compression waves. The compression waves again cross one another and are reflected on the boundaries of the jet as expansion waves.

As the flow changes direction along this boundary, many compression waves, formed at the interaction of expansion waves with the jet boundary, are sent back into the flow, these waves coalesce to from the intercepting shock in the interior of the jet. Along the central-line, where the expansion is a maximum, the pressure becomes so low relative to the ambient pressure that the recompression in the remaining cells reaches the limiting value for conical shocks, and the required compression takes place through an observable normal shock, properly termed Mach disc. Once the Mach disk forms the jet is said to be highly underexpnded. As the nozzle pressure ratio increases further the Mach disc increases both in strength and diameter.

Study of underexpaned jet involves calculation of jet boundary, intercepting shock, position of the first normal shock, and the cell length of repeating shock cell structures. The down-stream location of the Mach disk depends essentially on the static pressure ratio and the exit Mach number. The Mack disc location is increasing to the ratio of the specific heats, condensation, and solid boundary geometry at the nozzle lip.

If the pressure in the ambient medium to which is discharging is greater than the nozzle exits pressure ($p_e < p_a$), the jet is said to be overexpanded. In this, oblique shock waves are formed at the edge of the nozzle exit. These oblique shocks will be reflected as expansion waves from the boundary of the jet. Figure 1(c) schematically shows the waves prevailing in an over expanded jet. Due to this periodic shock cell structure is generated in the jet and the wave length of this periodic structure is found to increase with Mach number.

On passing through the shock from the opposite direction., it gets deflected as shown in the figure. The gas flow goes through these reflected shocks and is further compressed, but the flow is turned parallel to the centre line. This causes the pressure of the exhaust gas to increase the above ambient pressure. Deflected shock wave now hits the free boundary called a contact discontinuity or the boundary where outer edge of the gas flow meets the ambient atmosphere.

Pressure should be the same across the boundary and so as the direction of the flow. Since the jet is at a higher pressure than the ambient pressure, the pressure must reduce. Thus, at the reflected shock wave contact discontinuity interaction, the expansion waves of the Prandtl-Meyer type are generated to reduce the pressure come to an equilibrium with the ambient pressure. These expansion waves turn the flow away from the centreline. The expansion waves in turn deflect from the centre plane towards the contact discontinuity. The gas flow passing through the deflected expansion waves is now turned back parallel to the centre line but undergoes a further reduction of pressure. The deflected expansion waves now meet the contact discontinuity and reflect from the contact discontinuity toward the centre line as compression waves. This allows the gas flow to pass through the compression waves and increase its pressure to ambient pressure, but passes through the compression waves turns the flow back towards the centre line. The compression waves now deflect from the centre line as compression waves, further increasing the pressure above ambient, but turn the flow parallel to the ambient centre line. The flow process is now back to same that of the flow just passed through the reflected shock wave, i.e., the flow pressure is above the ambient pressure and the flow is parallel to the centre line. This process of expansion and compression wave formation continues until the pressure of the jet field becomes the same as the ambient pressure and the flow becomes parallel to the nozzle centre line. These expansion and compression waves which intact with each other lead to the formation of diamond patterns termed shock cells.

Immediately downstream of the Mach disc, the flow becomes subsonic, whereas the flow behind the shock that reflects from the interaction of the intercepting shock and Mach disc is still supersonic. Since the surrounding flow in the oblique shock region remains supersonic, a slip line exists at the boundary between the two concentric regions. For a fairly high degree of under expansion, say P_0/p_a = 4, this subsonic region quickly gets accelerated and becomes supersonic once again near the beginning of the second cell. In this case the second cell may resemble the first and even possess a Mach disc or normal shock similar to that in the first cell. For very high-pressure ratios, the structure downstream of the first cell is influenced for a large distance by the very strong normal shock Mach at the end of the cell, and no other normal shock is present. The flow then decays through oblique shocks and compression waves. The mixing region surrounds the core as usual, but the radial diffusion is small, with the result that the core of the highly underexpanded jet can be extremely long. The axial extent of the supersonic zone in the high-speed jet is a direct measure of the physical size of the jet core. The length is determined by the axial point farther downstream at which there exists a flow Mach number unity. Figure 1 (c) illustrated supersonic jets emanating at $p_e < p_a$ and it now known as overexpanded jets. Most of the flow characteristics is described above.

Settles and Hargather [22] and Settles [23] have presented a unified view of the history, rationale, applications, and current status of colour-coding schlieren optical techniques, based on an extensive literature review by them. The characteristics and advantages of colour flow visualization technique have been discussed in terms of colour-coding, qualitative and quantitative visualisations, and system sensitivity, range and resolution. Colour schlieren methods in shock wave research have been explained to visualize refractive index variations in transparent media by Kleine *et al.,*[24].

Present numerical studies evolved axisymmetric free jets exhausting from supersonic nozzles into still air. For jets exhausting into still air, consideration is given to the effects of jet Mach number, nozzle semi-divergence angle 15° (without flow separation inside nozzle), and jet static pressure ratio upon jet structure, and the shape and curvature of the jet boundary. The primary variables considered are exit jet Mach number, jet static pressure ratio and ratio of specific heats of the jet equal to 1.4. The simulation problem and the case of a hypothetical hypersonic vehicle are examined; A few flow field observations are included in conjunction with colour schlieren supersonic free jets employing image processing technique of MATLAB®.

Governing fluid dynamics equations

Effects of turbulence mixing, which can substantially change the flow far downstream of the nozzle exit plane, are neglected in the present numerical simulations. The assumption of large Reynolds number and low Knudsen number is relatively safe, except for the region in vicinity of jet boundary, where substantial mixing take place. Attributed to the highly nonlinear nature of these flows, the Euler equations give a reasonable model for the physics of fluids. To capture shocks and discontinuities, the time-dependent compressible axisymmetric Euler equations are written in conservation form as

$$\frac{\partial \boldsymbol{W}}{\partial t} + \frac{\partial \boldsymbol{F}}{\partial x} + \frac{1}{r}\frac{\partial (r\boldsymbol{G})}{\partial r} + \frac{\boldsymbol{H}}{r} = 0 \qquad (1)$$

where

$$\boldsymbol{W} = \begin{bmatrix} \rho \\ \rho u \\ \rho v \\ \rho e \end{bmatrix}, \boldsymbol{F} = \begin{bmatrix} \rho u \\ \rho u^2 + p \\ \rho uv \\ (\rho e + p)u \end{bmatrix}, \boldsymbol{G} = \begin{bmatrix} \rho u \\ \rho uv \\ \rho v^2 + p \\ (\rho e + p)v \end{bmatrix}, \boldsymbol{H} = \begin{bmatrix} 0 \\ 0 \\ p \\ 0 \end{bmatrix}$$

with the ideal gas assumption, the pressure and total enthalpy can be expressed as

$$\rho e = \frac{p}{(\gamma - 1)} + \frac{1}{2}\rho(u^2 + v^2) \qquad (2)$$

where γ is assumed to be 1.4.

Numerical scheme

The numerical algorithm employs finite volume discretization scheme. Spatial and temporal terms are decoupled applying method of lines. The computational region is divided into a number of quadrilateral grids. The conservative variable $\boldsymbol{W}$ within each grid is evaluated by their average value at quadrilateral grid centre. The inviscid flux vectors $\boldsymbol{F}$ and $\boldsymbol{G}$, and source vector $\boldsymbol{H}$ of Eq. (1) are evaluated on each side of the grid.

The above numerical scheme needs additions of artificial dissipation terms to preserve odd-even decoupling and to controlled numerical oscillations in vicinity of severe flow gradients. The blend of second and fourth differences provided third-order background dissipation in smooth regions of the flow and first-order dissipation in shock waves. Fourth-order dissipation is added everywhere in the computational region where the solution is smooth, but are ‘switch-off’ in the region of shock wave. The artificial dissipation model adopted in the present paper is based on the work of Jameson, Schmidt, and Turkel [25].

The spatial discretization described above reduces the governing fluid dynamics equations to semi-discretized ordinary differential equations. The integration is carried out using a two-stage Runge-Kutta time-stepping scheme [25]. In order to minimize the computation time, the evaluation of the dissipation term is carried out only at the first stage, and then frozen for the subsequent stages. The numerical scheme is stable for a Courant number ≤ 1. A local time step is used accelerate convergence to achieve steady state numerical solution by advancing the time step at each grid point with the maximum time step allowed by the local Courant–Friedrichs–Lewy (CFL) condition.

Boundary conditions

At the centre-line of the axisymmetric jet, a mirror image cell condition is applied to accommodate symmetric condition. At the downstream of the jet, all of the flow properties in the cell are extrapolated from the adjacent interior cells. At the nozzle exit plane, all of the flow variables are prescribed since the incoming flow is supersonic. For quiescent external condition, the ambient atmospheric condition is considered as the outer boundary condition of the jet. The outer boundary is taken about ten times the nozzle exit diameter d_e.

Computational domain

Supersonic jets exhausting into a normally stationary external stream are computed using inviscid flow solver developed inhouse. The initial jet radius is equal to the exit radius i.e. equal to $0.5d_e$. A simple algebraic grid generation program is used to generate computational grid in computational domain [26]. Due to axisymmetric nature of the problem, the computations are carried out on only one half of the jet. The computations were employed about 600 equally spaced grid points in the axial direction. A grid refinement was carried out in the radial direction by employing 60, 80, 100 and 120 mesh points. The present numerical simulation was carried out on 120 × 600 grid points which were selected after extensive grid independent test [21]. The convergence criterion to steady-state is taken (between two successive iterations) $|\rho^{n+1} - \rho^n| \leq 10^{-4}$, where n is an iterative index. The steady-state is achieved after about 50000 iterations. We have obtained Mach contour in the initial region of the convergent-divergent nozzle at M_e = 2.0 and 2.4 and semi-divergence angle of 15° as shown in Fig. 2(a) and (b), respectively, for P_o/p_a = 7. Primary purpose of this paradigm is to capture all the essential flow features using viscous flow solver as shown in Fig. 1. It is important to mention here that no flow separation is occurred in the divergent section of the nozzle at the semi-divergence angle of 15°.

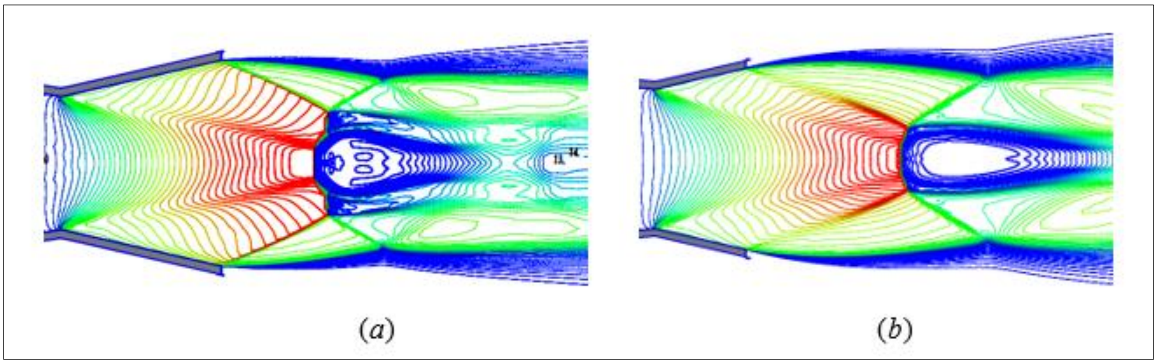

Fig. 2: Mach contour inside divergent section of convergent-divergent nozzle at (*a*) M_e = 2 and (*b*) M_e = 2.4

Experimental facility

All the experimental simulations of supersonic free jet were conducted in an Open Jet Facility as shown in Fig. 3. Air was obtained from a large storage system. The air used thus had a very low absolute humidity due to the high storage pressure. High pressure dry air at 4.3 × 10^6 Pa at ambient temperature was fed through a 15 × 10^{-3} m diameter pipe line to the settling chamber. The air leaving the storage system passed though valve, though the test nozzle assembly [27], and then discharge into the atmosphere. The pressure upstream of the test nozzle was maintained constant by a pressure regulating valve. The pressure in the settling chamber is continuously recorded and monitored using a Bourdon pressure gauge and a pressure transducer. The experimental set up is shown in Fig. 3 and connected with data acquisition. The open jet facility can be operated continuously at the maximum pressure up to about 80s. Pitot tube of 1.1 mm outer diameter is used for measuring the centre-line pressure.

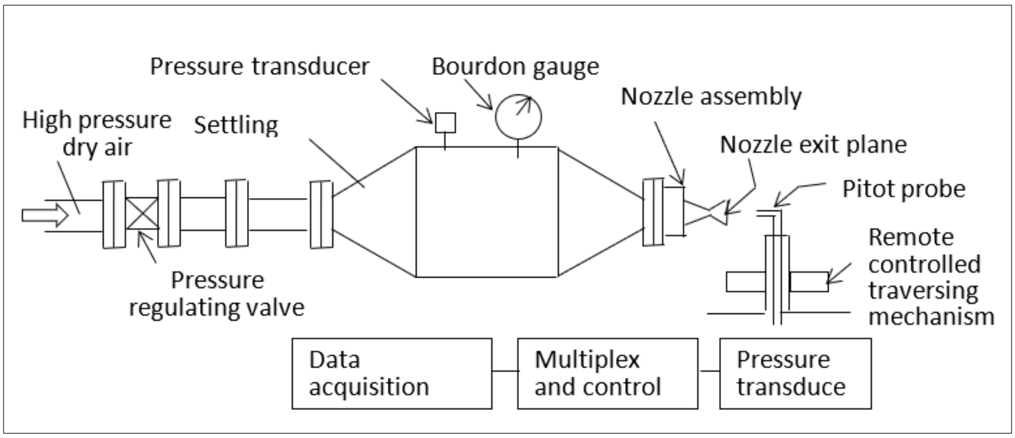

Fig. 3: Experimental set-up of open jet facility

RESULTS AND DISCUSSION

The flow does not separate in the nozzle for 15° semi-conical angle of nozzle and computed flow field is shown in Fig. 2. The above numerical algorithm is used to solve flowfields of free jets issuing from convergent-divergent nozzle at semi-divergence angle 15°. This semi-divergent angle no flow separation inside the nozzle. The exit nozzle Mach number M_e was computed by the isentropic flow relation [28]

$$\frac{A_e}{A^*} = \frac{1}{M_e}\left[\frac{2}{\gamma+1}\left(1+\frac{\gamma-1}{2}M_e^2\right)\right]^{\frac{\gamma+1}{2(\gamma-1)}} \quad (3)$$

Supersonic jet emanating from a convergent-divergent nozzle may be overexpanded ($p_e/p_a < 1$), correctly expanded ($p_e/p_a = 1$) or underexpanded ($p_e/p_a > 1$) depending upon ratio of stagnation pressure to ambient pressure (P_0/p_a). The following test cases as described in Table 1 were considered in the numerical simulation

Table 1: Nozzle dimension and operating parameters

d^*, mm	d_e, mm	A_e/A^*	M_e	Pressure ratio
2.18	30.0	2.005	2.20	$0.36 < p_e/p_a < 1.90$
9.2	15.72	2.923	2.61	$0.39 < p_e/p_a < 1.62$
10.66	23.0	4.657	3.12	$0.47 < p_e/p_a < 0.88$

The first two nozzles in the above Table 1 were operated at $p_e/p_a < 1$ as well as $p_e/p_a > 1$. The downstream location of the Mach disc, depends mainly on the p/P_o and M_e. Consider the flow at the lip of a nozzle with half angle θ. The flow properties change gradually and isentropically and called Prandtl-Meyer flow [28]

$$\nu = \sqrt{\frac{\gamma+1}{\gamma-1}}\tan^{-1}\sqrt{\frac{\gamma+1}{\gamma-1}(M^2-1)} - \tan^{-1}\sqrt{M^2-1} \quad (4)$$

The Prandtl-Meyer angle ν, which can be calculated, is the angle through which sonic flow turns to attain a supersonic Mach number M. The Prandtl-Meyer angle ν, which can be calculated, is the angle through which sonic flow turns to attain a supersonic Mach number M.

At the nozzle lip, before expansion, the Mach number M_j and corresponding Prandtl-Meyer angle is ν_j. After expanding to atmospheric pressure, the Mach number is M_e with corresponding Prandtl-Meyer angle becomes ν_j. Thus, the flow at the nozzle lip turns through an angle of ($\nu_j - \nu_e$) relative to the nozzle wall, and the overall flow expansion angle with respect to the flow axis is α.

$$\alpha = (\nu_j - \nu_e) + \theta \quad (5)$$

The Prandtl-Meyer angle ν, which can be calculated as the angle through which sonic flow turns to attain a supersonic Mach number M. When a M_j expands to a M_e, according to a Prandtl-Meyer expansion, the turning angle is ($\nu_j - \nu_e$). Hence the Prandtl-Meyer flow turned $\Delta\nu = \pm\delta$, and α is the turning streamline. Figure 4 delineated all above symbols at the lip of the nozzle including total angle turned through by the flow at the lip of an underexpanded nozzle, in terms of nozzle and Prandtl-Meyer turning angle. The flow to turned from initial expansion angle by the intersection of expansion waves with the boundary reflecting as compression waves so that the condition of constant pressure boundary is satisfied at every point. Immediately after leaving the nozzle exit, then, the flow at the nozzle lip has turned through the total angle.

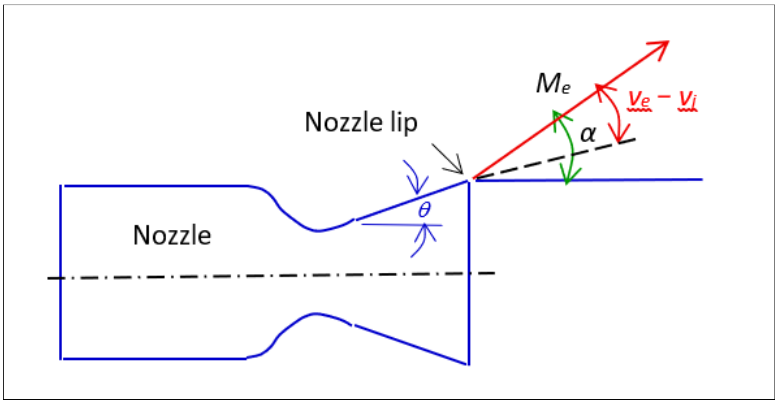

Fig. 4: Total angle turned at the lip of under expanded nozzle in terms of Prandtl-Meyer turning angles

Schlieren flowfield

The computed flowfields observed through the density contours are shown in Figs. 5 (a, b, c) for M_e = 2.20, 2.61 and 3.12 respectively. All the discontinuities like jet shock, triple point, slip lines, reflected shock and shock cells are clearly visible as sketched in Fig. 1. It was possible to measure shock cell lengths (L_1, L_2, L_3 and L_4) and the location of the Mach disc (L_m) from the nozzle exit from these. Figure 6 (a, b, c) depicts corresponding schlieren photographs [27]. The shock-cell spacing were directly measures from the schlieren pictures. All the discontinuities are clearly visible in the pictures.

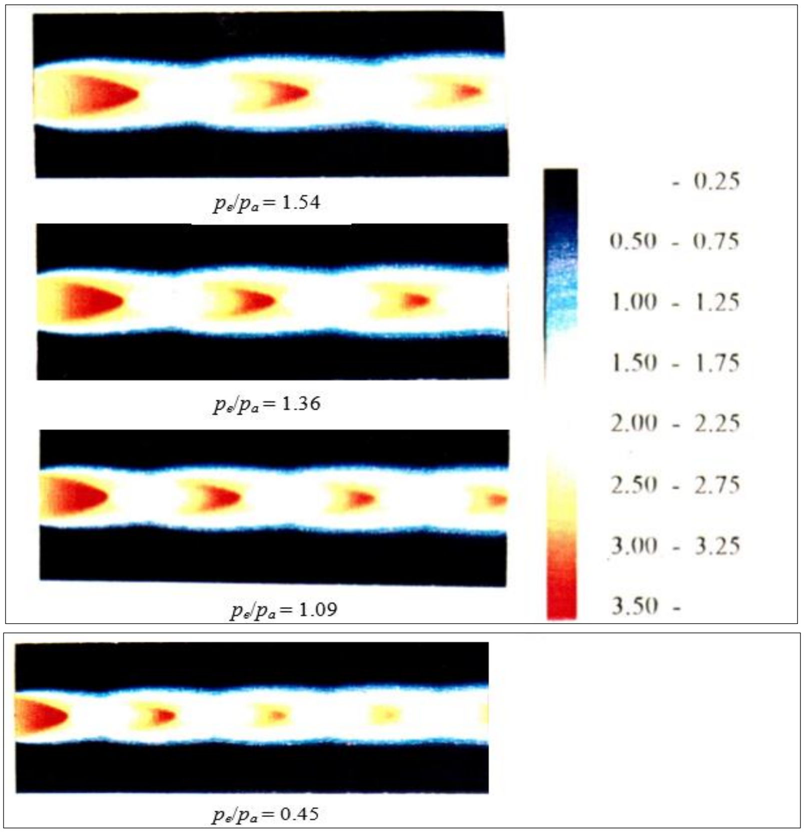

Fig. 5a: Density contour for M_e = 2.20

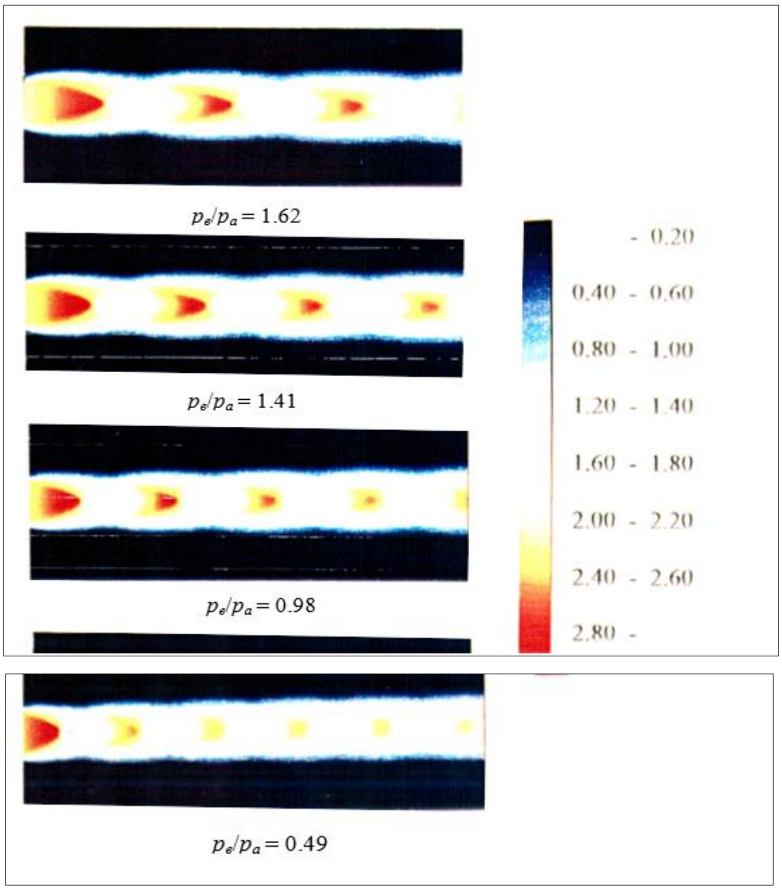

Fig. 5b: Density contour for M_e = 2.61

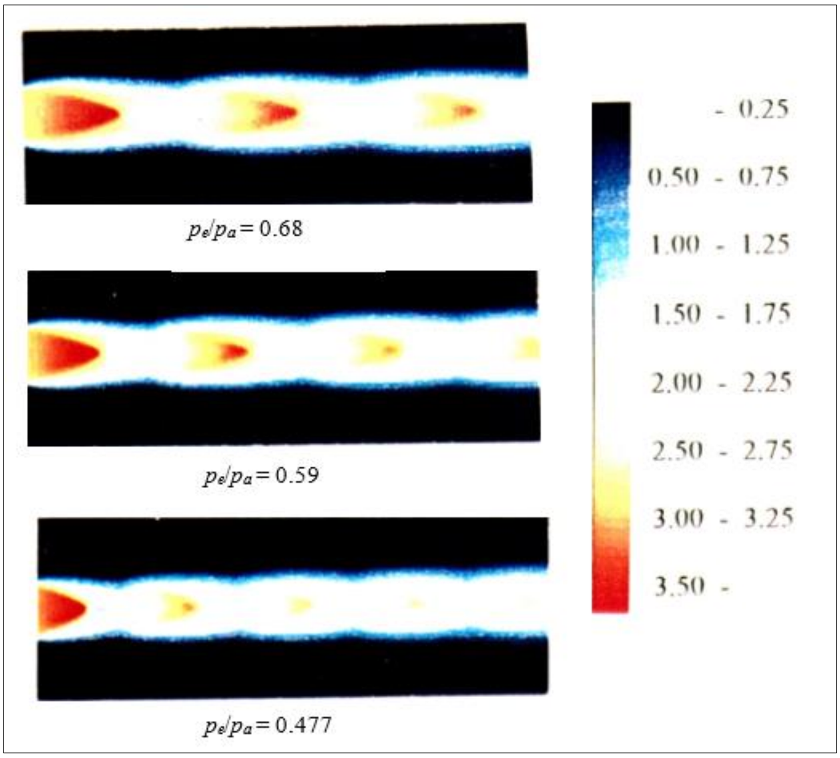

Fig. 5c: Density contour for M_e = 3.12

Mach disc location L_m, first, second and third shock cell length L_1, L_2, L_3 and L_4 respectively are calculated and measured from density contours (Fig. 5) and schlieren pictures (Fig. 6). Mach disc location L_m compared with [27], first, second and third shock cell length L_1, L_2, and L_3, are compared with Abdel-Fattah

[14]. The Mach contours are showing good agreement with the schlieren pictures [27].

First shock cell length

The comparison of L_1 obtained through the present numerical studies and that of Abdel-Fattah [14] and Chattopadhy *et al.,* [27] is shown in Fig. 7. The value of shock strength is defined as

$$\beta^2 = (M_e^2 - 1) = \left(\frac{2}{\gamma-1}\right)\left(\frac{p_o}{p_e}\right)^{\frac{\gamma+1}{2}} - \left(\frac{\gamma+1}{\gamma-1}\right) \quad (6)$$

for imperfectly expended supersonic jets, $p_e/p_a \neq 1$ supersonic jets relation given by Tam and Tanna [29] was adopted

$$\frac{d_j}{d_e} = \sqrt{\frac{M_e}{M_j}}\left[\frac{1+\frac{1}{2}(\gamma-1)M_j^2}{1+\frac{1}{2}(\gamma-1)M_e^2}\right]^{\frac{\gamma+1}{4(\gamma-1)}} \quad (7a)$$

$$\frac{\Delta p}{p_a} = \left[\frac{1+\frac{1}{2}(\gamma-1)M_j^2}{1+\frac{1}{2}(\gamma-1)M_e^2}\right]^{\frac{\gamma}{(\gamma-1)}} - 1 \quad (7b)$$

$$\frac{p_e}{p_a} = \left[\frac{1+\frac{1}{2}(\gamma-1)M_j^2}{1+\frac{1}{2}(\gamma-1)M_e^2}\right]^{\frac{\gamma}{(\gamma-1)}} \quad (7c)$$

where $\Delta p = \pm(p_e - p_a)$ is positive or negative for under expanded and over expanded condition respectively. Similar calculations were done with the test results of $M_e = 2.2$ and the plotting of L_1/d^* vs β^2 shows the linear relationship for over expended conditions. However, the slope has decreased because the M_e decreased. Results for $M_e = 3.1$ are shown in the same Fig. 7. It was operated in the overexpanded region and it also shows same linear variation of L_1/d^* with β^2. The slope of the curve has increased compared to the previous nozzles due to the increase in M_e of the nozzle. L_1/d^* varies linearly with β^2 for $p_e/p_a < 1$ and shows good agreement with the result of Abdel-Fattah [14]. A least square straight line fit from these data indicated

$L_1/d^* = 1.04\,\beta^2 - 1.08$ for $M_e = 2.2$ $(1.03 < \beta^2 < 3.84)$ (8a)
$L_1/d^* = 1.15\,\beta^2 - 1.95$ for $M_e = 2.6$ $(1.70 < \beta^2 < 5.81)$ (8b)
$L_1/d^* = 1.25\,\beta^2 - 3.85$ for $M_e = 3.1$ $(3.08 < \beta^2 < 8.70)$ (8c)

Hence using these relations, it is possible to find out the length of first shock cell L_1 for these Mach numbers. Comparison of L_1/d^* for $M_e = 2.61$ shows good agreement with Abdel-Fattah [14]. It is observed from Fig. 7 that L_1/d^* varies linearly with β^2 for the underexpanded condition.

Second shock cell length

The measurement of L_2 was carried out in the similar way and shown in Fig. 8. The comparison of the results with that of Abdel-Fattah [14] are also shown. The results of the above references show linear variation of L_2/d^* with β^2 for $M_e = 2.6$ and 2.85 according to the following equation

$L_2/d^* = 0.87\,\beta^2$ for $M_e = 2.6$ $(1.03 < \beta^2 < 3.84)$ (9)

From the present studies, it is seen that the results of $M_e = 2.2$, 2.6 and 3.1 fall on the same curve. This indicates that the L_2 nondimensional with d^*, varies linearly with β^2 for all nozzle irrespective of the M_e. The L_2/d^* varies linearly with β^2 for all the nozzles irrespective of M_e. In general, it is observed that $L_1 > L_2$ for $p_e/p_a > 1$ and $L_1 = L_2$ for $p_e/p_a = 1$ and $L_1 < L_2$ for $p_e/p_a < 1$.

Third and fourth shock cell lengths

From the photographs it was possible to measure L_3 and L_4 only in the overexpanded case where it was distinctly visible. However, in the underexpanded cases it was not possible to visualize due to the limitation of the size of the mirror. It is found that from the schlieren pictures is found about $L_3 = 0.94L_2$ and $L_4 = 0.87L_2$ which closely agree with the results of [14].

The L_2/d^* varies linearly with β^2 for all the nozzles irrespective of M_e. in general, it is observed that $L_1 > L_2$ for $p_e/p_a > 1$ and $L_1 = L_2$ for $p_e/p_a = 1$ and $L_1 < L_2$ for $p_e/p_a < 1$. From the schlieren pictures is found about $L_3 = 0.94\,L_2$.

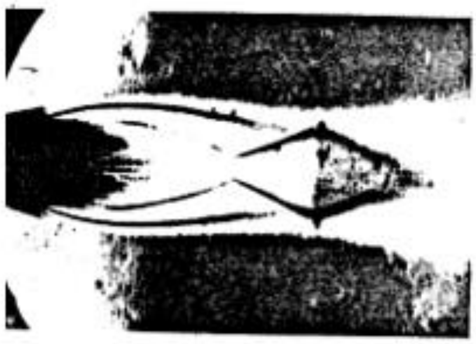

$p_a/p_e = 1.56$

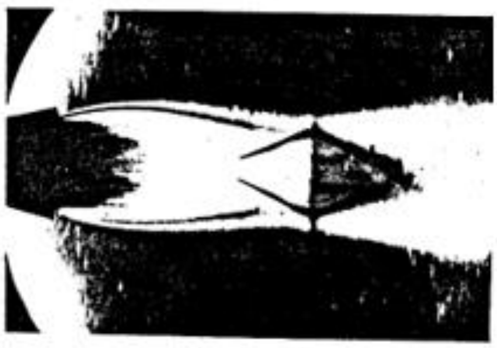

$p_a/p_e = 1.36$

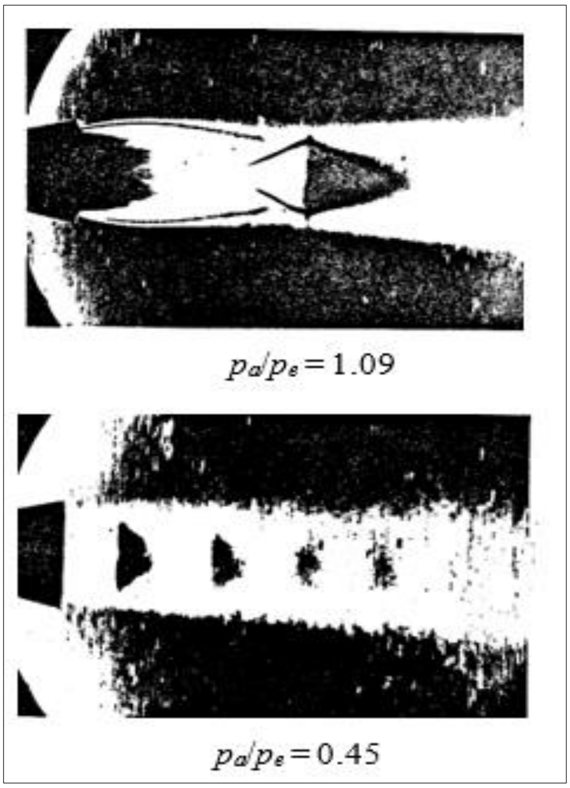

Fig. 6a: Schlieren flow field visualization M_e = 2.20

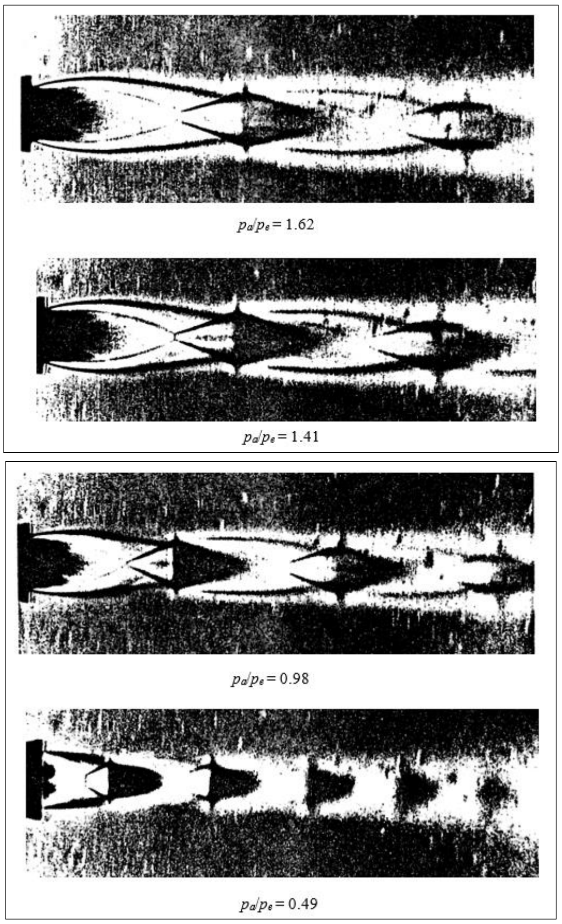

Fig. 6b Schlieren flow field visualization M_e = 2.61

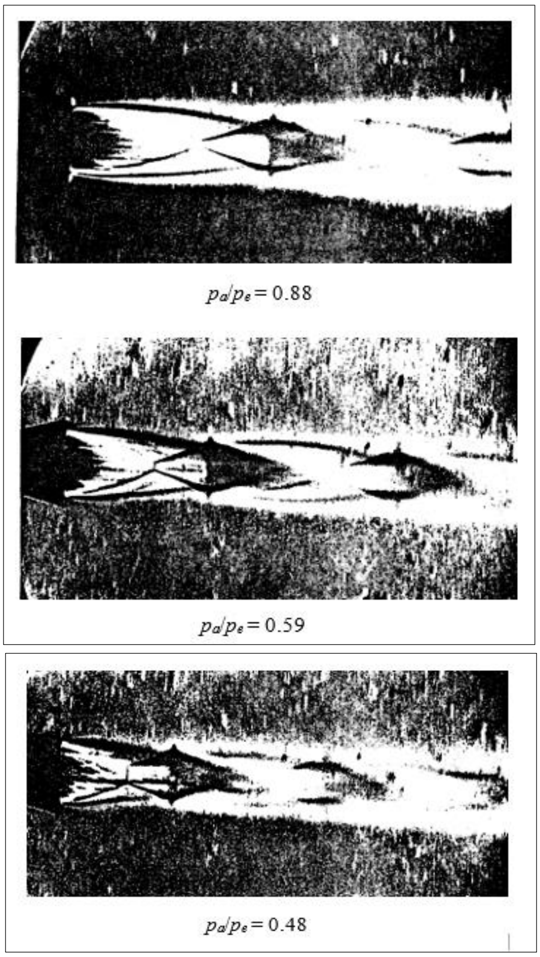

Fig. 6c Schlieren flow field visualization M_e = 3.12

Mach disc location

Figure 9 Variation of shock cell length versus shock strength for various M_e. The location of Mach disk moves away from the nozzle exit plane with increase in expansion pressure ratio p_e/p_a. For p_e/p_a < 1 cases, the strong jet shocks from the nozzle forms the Mach disc very near to the nozzle exit; hence the estimation of Mach disc location becomes difficult.

The numerical and experiments are conducted at ambient temperature and data are available in the form of Mach contour schlieren pictures and surface pressure and pitot pressure along the jet axis. It is observed that the location of Mach disc obtained agree well with available experimental data of [27]. An overexpanded nozzle ($p_e < p_a$) leads to oblique shock waves at the exit of the nozzle which intersect and give the familiar "diamond" pattern. If the degree of overexpansion is great enough, this pattern is modified so as to terminate the oblique shocks with a normal shock or the so-called Mach disc configuration. On the other hand, a sufficiently underexpanded nozzle will lead to a similar Mach disc because of the focusing of compression waves from the jet boundary. At extreme degrees of underexpansion, the oblique shocks and their reflection from the Mach disc are markedly curved, and the configuration is appropriately termed a shock bottle.

Pressure distributions along the jet axis

Figure 10(a) shows the results obtained for M_e = 2.2 at p_e/p_a = 1.2 and compared the results of [27]. Similarly, Fig. 10(a) shows the comparison of the results of the same nozzle at p_e/p_a =1.0 with the results of [28]. Fairly good agreement is found up to x/d_e = 4.0 for p_e/p_a = 1.2 and up to x/d_e = 2.2 for p_e/p_a =1.0. the difference in values at x/d_e = 4.0 arises due to the presence of nozzle shock. The location of Mach disc is clearly indicated and is in good agreement with that observed in Mach contour and schlieren photographs in Figs. 5 and 6, respectively.

Table 2 Shock cell lengths in supersonic free jets

P_o/p_a	p_e/p_a	β^2	M_j^2	L_1/d^*		L_2/d^*		L_3/d^*	
				Measured	Calculated	Measured	Calculated	Measured	Calculated
M_e = 2.20									
12.88	1.2	4.36	5.36	3.1	3.7	3.1	4.1	2.7	2.6
10.69	1.0	3.84	4.84	2.9	3.0	2.4	3.6	2.4	2.2
8.55	0.8	3.23	4.23	2.4	2.5	2.7	3.1	2.4	2.0
6.47	0.6	2.50	3.50	1.8	1.8	1.8	2.4	1.8	1.6
M_e = 2.61									
23.95	1.2	6.38	7.38	4.7	5.0	4.2	5.9	-	-
19.95	1.0	5.76	6.76	4.2	4.3	3.7	5.2	-	-
15.55	0.8	5.03	6.03	3.2	3.7	3.7	4.6	3.3	-
11.97	0.6	4.16	5.16	2.6	2.7	2.9	4.6	3.2	-
M_e = 3.1									
25.59	0.8	7.70	8.70	5.4	5.7	5.4	6.8	-	-
19.12	0.6	6.62	7.62	4.0	4.7	4.7	5.9	4.2	-
17.09	0.4	5.24	6.24	3.3	3.2	3.3	4.8	3.3	-

The pressure distribution at p_e/p_a = 0.8 and 0.6 is shown in Fig. 10(b), respectively. It can be seen that the trend is almost similar. However, the location of the Mach disc moves towards the nozzle exit with decrease in p_e/p_a as well the shock cell length. However, in the range of present study, it was found that at p_e/p_a = 0.6 the pitot pressure has gone up to the maximum value at a distance around x/d_e = 4.5. The location of maximum pitot pressure increases with the increase in expansion ratio. This indicates that flame deflector tests should be carried out at different range of stand-off distances depending upon the expansion ratio p_e/p_a of the nozzle. The arrows marked in Fig. 10 indicate the location of Mach disc on jet axis.

Mach distribution along the jet axis

Mach number distribution up to the location of Mach disc is obtained using measured values of Pitot pressure p_{t2} and settling chamber pressure P_o. Using the following relation [28] which the following relation which is under the assumption that the flow is isentropic

$$\frac{p_{t2}}{p_s} = \left[1 + \frac{(\gamma-1)}{2} M^2\right]^{\frac{\gamma}{\gamma-1}} \qquad (10)$$

and

$$\frac{p_{t2}}{p_s} = \left[\frac{(\gamma+1)M^2}{2}\right]^{\frac{\gamma}{\gamma-1}} \left[\frac{(\gamma+1)}{2\gamma M^2-(\gamma-1)}\right]^{\frac{1}{\gamma-1}} \qquad (11)$$

It can be seen that the pressure distribution shows the repetitive structures as observed in the schlieren photograph. The pressure distribution it is possible to estimate the flow Mach number up to the location of Mach disc. For this, the value of pitot pressure, settling chamber pressure, along with the above Rankine-Huguenot relationship was used to estimate Mach number. The obtained result for M_e = 2.2 at p_e/p_a = 1.2 is shown in Fig. 11.

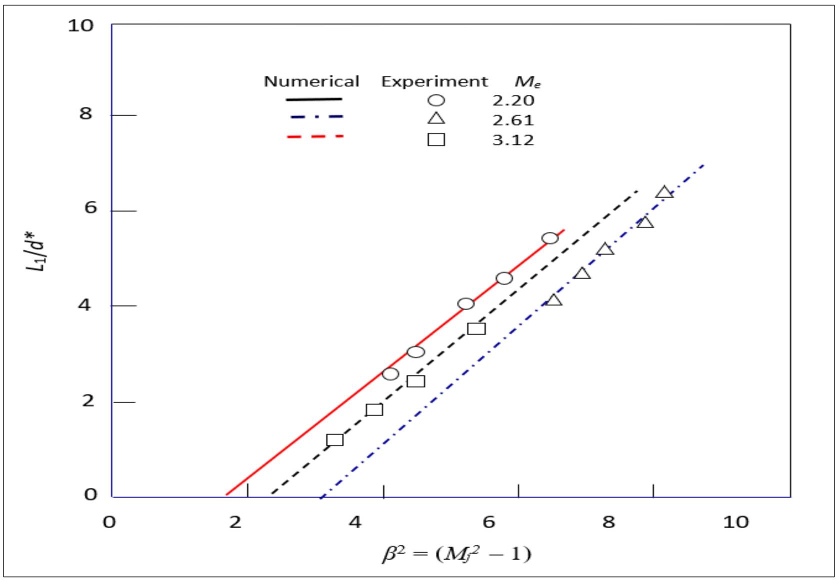

Fig. 7: Variation of first shock cell length versus shock strength for various M_e

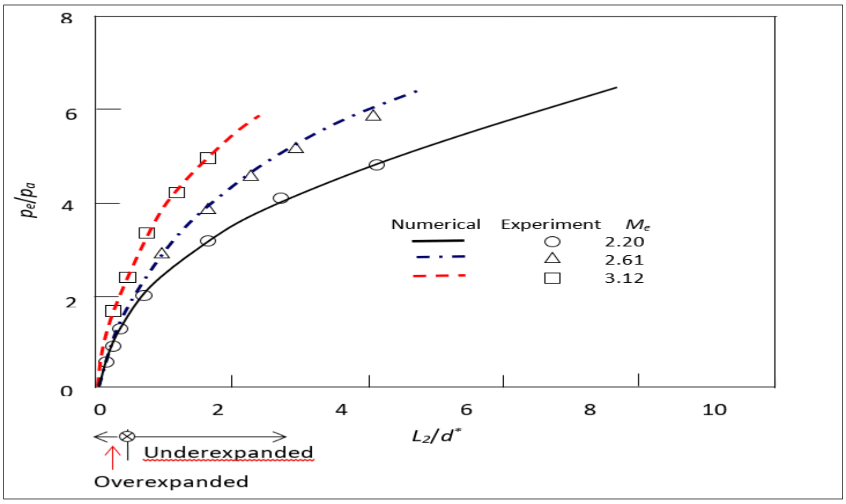

Fig. 8: Second Mach disc location versus pressure ratio at different M_e

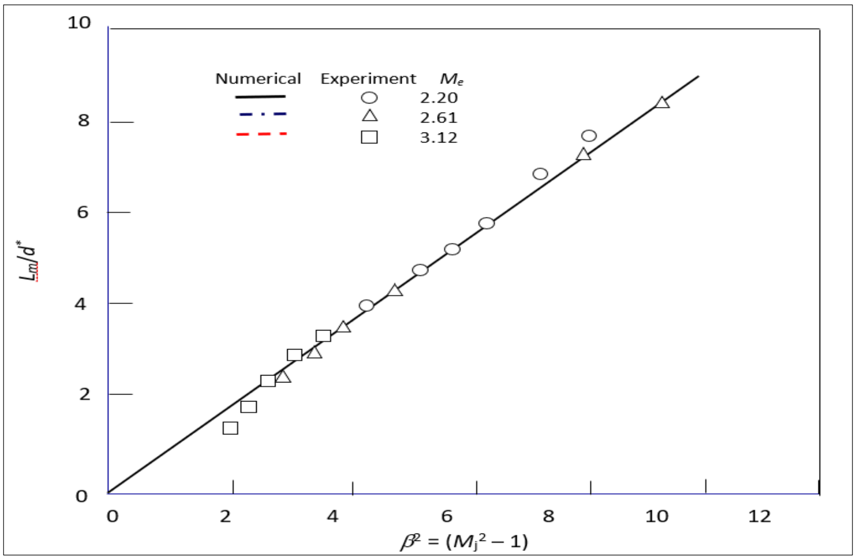

Fig. 9: Variation of shock cell length versus shock strength for various M_e

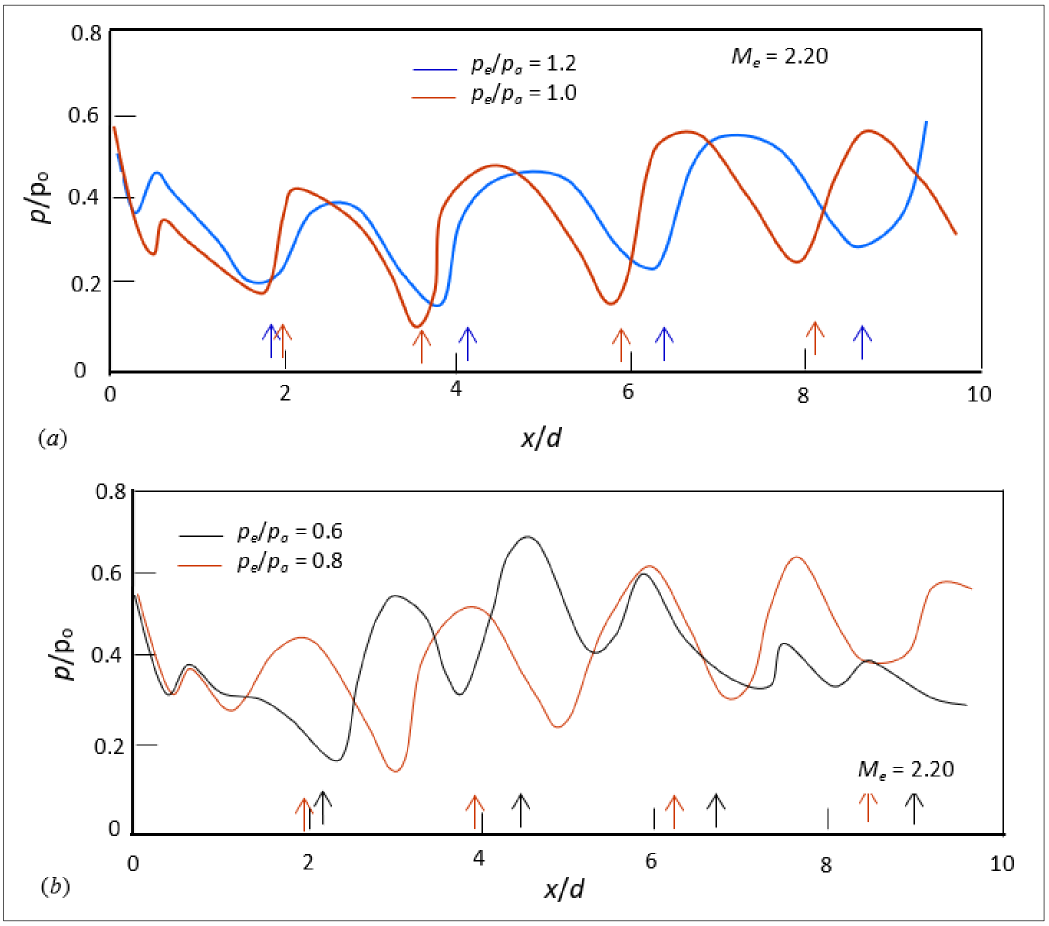

Fig. 10: Centre line pressure distributions along free jet (*a*) p_e/p_a = 1.2, 1.0 and (*b*) p_e/p_a = 0.6, 0.8

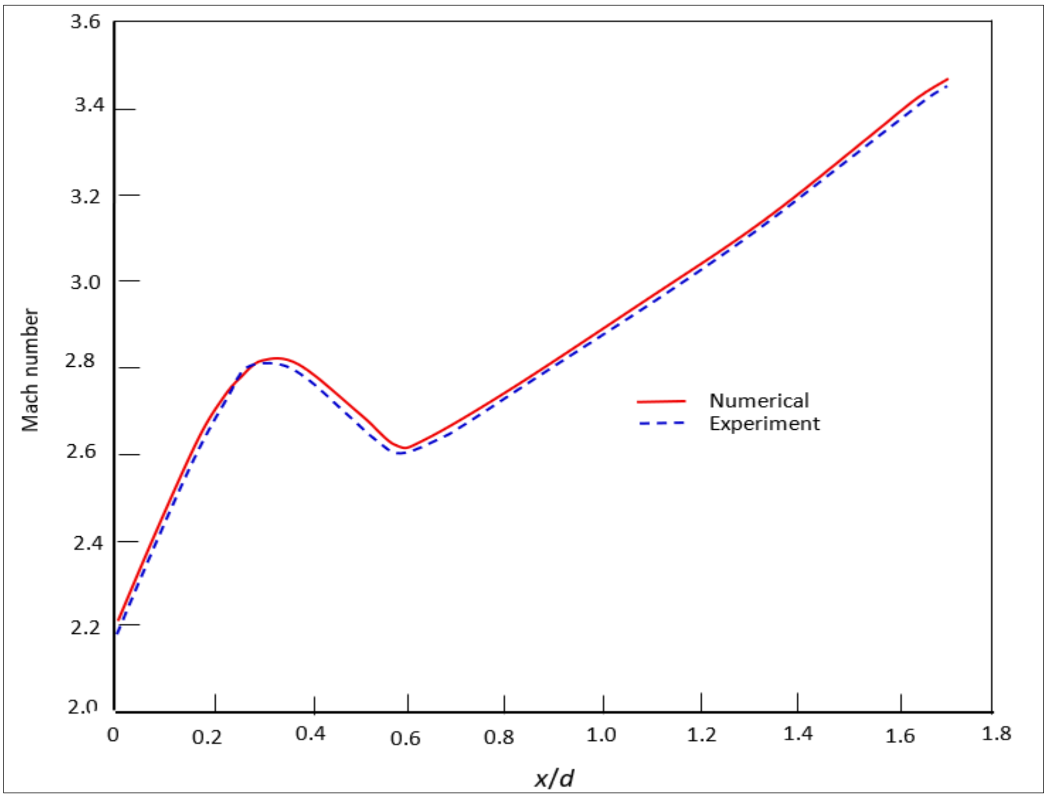

Fig. 11: Mach distributions along the centre line of supersonic free jets

Colour schlieren photograph

Schlieren methods are widely known and well established to visualize refractive index variations in transparent media. The use of colour allows one to obtain more data and previously inaccessible information from a picture taken with this technique. In general, a hue can be related to a certain strength or a certain direction of a refractive index gradient. While the first case essentially corresponds to the usual black- and-white system the latter correlation cannot be made adequately evident without the use of colour. Two colour schlieren techniques are presented here, which reach or even exceed the quality and sensitivity range of conventional black- and-white methods.

For colour schlieren photograph, a dispersion prism instead of colour gratings has been used to capture compression/expansion of the flow. Figure 12 shows spectrum of visible light. Hence different colours are observed provided by the spectrum of white light. Green has been selected as the background colours. Yellow, orange and red colours indicate compression in the increasing order, whereas blue to violet indicate expansions. Most of the features like expansion near the jet exit, jet boundary, jet shock, Mach disk, triple point, slip line, reflected shock, body shock (very weak in this case), expansion and compression of flow near the model surface, wall jet, etc., are clearly observed. This photograph (Fig. 13) clearly shows the complexity of flowfield.

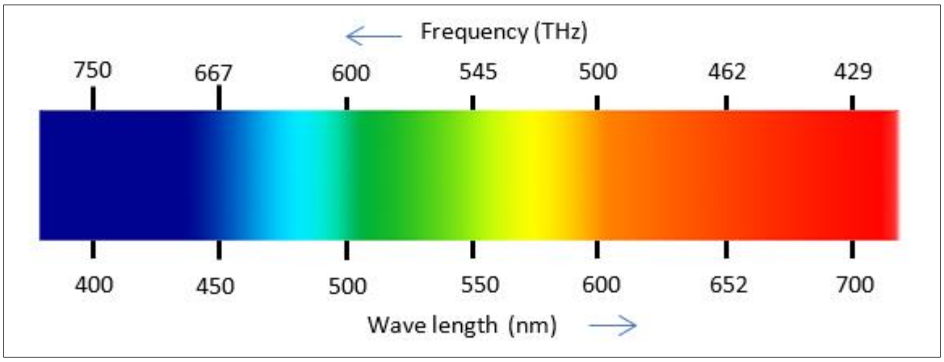

Fig. 12: Spectrum of visible light (prism)

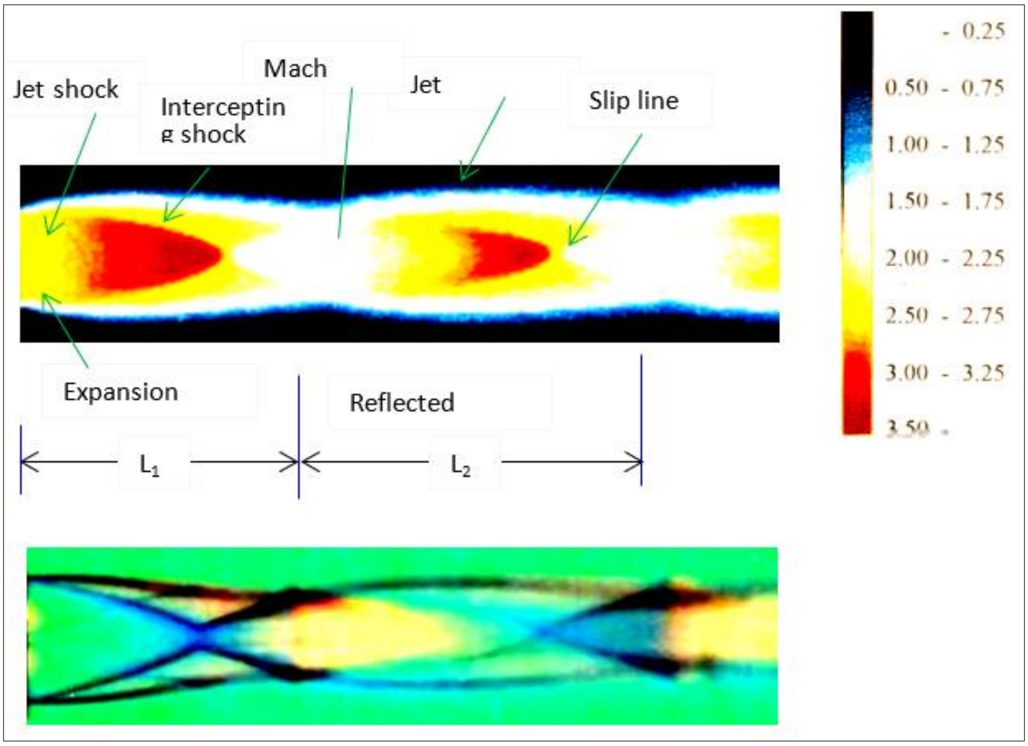

Fig. 13: Comparison between CFD with colour schlieren picture for free jets at p_e/p_a = 1.2 and M_e = 2.20

Figure 13 shows comparison between CFD with colour schlieren picture for free jets at $p_e/p_a = 1.2$ and $M_e = 2.20$. The various techniques for introducing colour into a schlieren system were explored, and all of them were found to have drawbacks such that the added dimension of colour in a schlieren has never been utilized for extensive quantitative measurements. An entirely new technique using a diffraction grating to produce the colour has been introduced as a modification of the conventional schlieren system. It provides solutions to the problems of sensitivity, range of measurement deflection and undesirable effects of diffraction which have limited the usefulness of colour systems in the past. Methods for analysing a conventional schlieren have been modified for the analysis of a colour schlieren result. Flowfield analysis for free jets shapes have been used obtained colour schlieren techniques in conjunction image processing algorithm based on MATLAB as described ln Ref. [30].

CONCLUSIONS

The scheme presented in this paper deals with the strong shocks that occur in supersonic jets, and captures the disparate-strength features well. The resulting flows show complex shock/shear/expansion structures, with Mach discs forming at high total pressure ratios, and the position of the Mach disc sensitive to the Mach number of the jet M_e. The shock cell lengths for free jet structures are obtained at different exit Mach numbers and expansion ratios. The data up to ten times the nozzle diameter has been obtained in the numerical simulations.

It is seen that the location of the Mach disc obtained from the present studies at M_e = 2.20, 2.61 and 3.12. At M_e = 2.20, it is good agreement with the results of for p_e/p_a = 1.2, and with the results of [27] for p_e/p_a = 1.0. The comparison of the shock cell lengths with the results of [14] for M_e = 2.62 are found to be in good agreement. For M_e = 3.12 the data have been generated and similar trends followed by it. This indicates that the length of first shock cell L_1 is a function of shock strength $\beta^2 = (M_j^2 - 1)$ and design Mach number M_j of a nozzle, however the length of the second cell L_2 is independent of M_j.

Nomenclature

A_e Nozzle exit cross-sectional area
A^* Nozzle throat area
d_e nozzle exit diameter
d_j effective jet diameter
d^* Nozzle throat diameter
e specific total internal energy
$\boldsymbol{H}$ source vector
$\boldsymbol{F}$, $\boldsymbol{G}$ inviscid flux vector
M_e exit nozzle design Mach number
M_j fully expanded jet Mach number
P_o stagnation pressure
p pressure
p_e pressure at the nozzle exit
p_a ambient static pressure
p_{t2} Pitot pressure measured along the centre line of jet
L_m Mach disc location
L_1 First shock cell length
L_2 Second shock cell length
L_3 Third shock cell length
L_4 Fourth shock cell length
x Axial distance from the nozzle exit plane
u, v velocity components in axial and radial direction, respectively
$\boldsymbol{W}$ Conserved vector quantities
β^2 shock strength, $(M_j^2 - 1)$
ρ density
θ Nozzle semi-cone angle
γ Ratio of specific heats

REFERENCES

1. Love, E. S. and Lee, L. P., Shape of initial portion of boundary of supersonic axisymmetric free jets at large jet pressure ratios. NACA TN 4195, 1958.
2. Love, E. S., Grigshy, C. E., Lee, L. P. and Wooding, M. J., Experimental and Theoretical Studies of Axisymmetric Free Jets. NASA TRR-6, 1959.
3. Wilcox, D. E., Weir, A., Nicholls, J. A. and Dunlop, R., Location of Mach disc and diamonds in supersonic air jets, Journal of the Aeronautical Sciences, **24**(2), 1957, pp. 150-152.
4. Madhu, B.P., Mahendramani, G. and Bhaskar, K., Numerical analysis on flow properties in convergent – Divergent nozzle for different divergence angle, Materials today Proceedings, 24(1) 2021, pp.207-215. https://doi.org/10.1016/j.matpr.2020.10.419
5. Mehta R. C. and Prasad J. K., Estimation of shock cell structure of axisymmetric supersonic free jets, Indian Journal of Engineering and Material Sciences. 3; 1993, pp. 141-147.
6. Zang, B., Vevek, U. S., Lim, H. D., Wei, X. and New, T. H., An assessment of OpenFOAM solver on RANS simulations of round supersonic free jets, Journal of Computer Science, **28**, 18–31 (2018). https://doi.org/10.1016/j.jocs.2018.07.002
7. Lohia, D. K., Kumar, B., Srivastava, S. and Paliwal, H. K., Numerical simulation of supersonic overexpanded jet from 2-D convergent-divergent nozzle, Int. J. Integr. Eng. **10**(8), 195–201 (2018). https://doi.org/10.30880/ijie.2018.10.08.029
8. Prandtl L., Über die stationären Wellen in einem Gasstrahl, Phys. Zeit. 5. Jahrgang, No. 19. pp. 599–601, 1904.
9. Powell A., On Prandtl's formulas for supersonic jet cell length. International Journal of Aeroacoustics. 2010;**9**(1-2):207-236. doi:10.1260/1475-472X.9.1-2.207
10. Chang, I. S. and Chow, W. L., Mach disc from underexpanded nozzle flow, AIAA Journal, 12(8) 1974, pp. 1079-1082.
11. Harper-Bourne, M. and Fisher, M. J., The noise from shock waves of supersonic jets, AGARD-CP, 131, 1972, pp. 1-19.
12. Perumal A. K. and Rathakrishnan, E., Scaling law for shock-cell length and its correlation with shock-associated noise of circular and elliptic supersonic free jets, Physics of Fluids **33**, 096103 (2021), https://doi.org/10.1063/5.0066026
13. Faheem, M., Khan, A., Kumar, R., Khan, S. A., Asrar, W. and Sapardi, M. A. M., Estimation of Mach numbers in supersonic jets using schlieren

images, Materials today Proceedings 24(7) 2021, pp. 2673-2676. doi.org/10.1016/j.matpr.2021.02.361
14. Abdel-Fattah A. M., Discrete tone emission from high-pressure ratio supersonic jets from convergent-divergent nozzles, AIAA Journal, **26**, 1988, 283-291 doi.org/10.2514/3.9886
15. Mehta R. C. and Prasad J. K., Investigation of supersonic free jets emanating from convergent-divergent nozzles, International Journal of Computational Fluid Dynamics, **10**, 1998, pp. 81-71. doi.org/10.1080/10618569808961673
16. Franquet, E., Perrier, V., Gibout, S. and Bruel, P., Free underexpanded jets in a quiescent medium: A review, Progress in Aerospace Sciences, **77**, 25–53 (2015). https://doi.org/10.1016/j.paerosci.2015.06.006
17. Munday, D., Gutmark, E. J., Liu, J. and Kailasanath, K., Flow Structure of Supersonic Jets from Conical C-D Nozzles, AIAA 2009-4005, DOI: 10.2514/6.2009-4005
18. Xiao, L., Hao, X., Lei, L., Tiezhi, S., Flow structure and parameter evaluation of conical convergent–divergent nozzle supersonic jet flows, Physics of Fluids 35, 066109 (2023), https://doi.org/10.1063/5.0151556
19. Yu, H., Lu, X., Lin, J., Zhang, B. and Zhao, Y., A Study on flow characteristics of supersonic annular centripetal convergent jet subjected to different nozzle pressure ratios, to be appeared in Physics of Fluids, 2025.
20. Meyer, T., Über zweidimensionale Bewegungsvorgänge in einem Gas, das mit Überschallgeschwindigkeit strömt. Ph.D. dissertation. Georg-August Universität, Göttingen. 1908.
21. Mehta, R. C., Analysis of Supersonic Free Jets and Impinging Supersonic Jets, Simulation Modeling, Recent Advances, New Perspectives, and Applications, 2024 DOI: 10.5772/intechopen.1002372
22. Settles, G. S. and Hargather, M. J., A review of recent developments in schlieren and shadowgraph techniques, Measurement Science and Technology, 28, 2017, 042001. doi:10.1088/1361-6501/aa5748
23. Settles, G.S., Colour-coding schlieren techniques for the optical study of heat and fluid flow, International Journal of Heat and Fluid Flow, Volume 6, Issue 1, March 1985, Pages 3-15 https://doi.org/10.1016/0142-727X(85)90024-4
24. Kleine, H. and Grönig, H. Colour schlieren methods in shock wave research. Shock Waves, **1**, 1991, pp. 51–63. https://doi.org/10.1007/BF01414868
25. Jameson, A., Schmidt, W., and Turkel, E., Numerical Simulation of Euler Equations by Finite Volume Methods Using Runge-Kutta Time Stepping Schemes, AIAA paper 81-1259, June 1981.
26. Mehta, R. C., Multi-Block Structured Grid Generation for Computational Fluid Dynamics, Scholar Journal of Engineering and Technology, **5**(8), 2017, pp. 387-219 DOI: 10.21276/sjet
27. Chattopadhya, S., Jacob, V. and Prasad, J. K., Supersonic free jet structure an experimental observation in open jet facility, Vikram Sarabhai Space Centre, Trivandrum, ATTF-R8, 1989.
28. Ames Research Staff, Equations, tables and charts for compressible flow, NACA report 1135, 1953.
29. Tam, C. K. W. and Tanns, H. K., Shock associated noise of supersonic jets from convergent-divergent nozzles, Journal of Sound and Vibration, 81, 1982, pp. 337-358
30. Alsiya, S., Jey Lekshmi, C., Jishna Priya, B. P. and Mehta, R. C., Image processing algorithm for fringe analysis in photoelasticity, Scholar Journal of Engineering Technology, 4(7) 2026, pp. 325-328. DOI: 10.21276/sjet.2016.4.7.5